ACS APPLIED MATERIALS & INTERFACES

Research Article

www.acsami.org

Flexible and Transparent Metallic Grid Electrodes Prepared by Evaporative Assembly

Jae Hoon Park,[†,#] Dong Yun Lee,[∥,#] Young-Hoon Kim,[⊥] Jung Kyu Kim,[†,‡] Jung Heon Lee,[†,§] Jong Hyeok Park,[†,‡] Tae-Woo Lee,[⊥] and Jeong Ho Cho*[,†,‡]

[†]SKKU Advanced Institute of Nanotechnology (SAINT), [‡]School of Chemical Engineering, [§]School of Advanced Materials Science and Engineering, Sungkyunkwan University, Suwon 440-746, Republic of Korea

[∥]Materials Research Center, Samsung Advanced Institute of Technology (SAIT), Suwon 443-803, Republic of Korea

[⊥]Department of Materials Science and Engineering, Pohang University of Science and Technology (POSTECH), Pohang 790-784, Republic of Korea

Supporting Information

ABSTRACT: We propose a novel approach to fabricating flexible transparent metallic grid electrodes via evaporative deposition involving flow-coating. A transparent flexible metal grid electrode was fabricated through four essential steps including: (i) polymer line pattern formation on the thermally evaporated metal layer onto a plastic substrate; (ii) rotation of the stage by 90° and the formation of the second polymer line pattern; (iii) etching of the unprotected metal region; and (iv) removal of the residual polymer from the metal grid pattern. Both the metal grid width and the spacing were systematically controlled by varying the concentration of the polymer solution and the moving distance between intermittent stop times of the polymer blade. The optimized Au grid electrodes exhibited an optical transmittance of 92% at 550 nm and a sheet resistance of 97 Ω/sq. The resulting metallic grid electrodes were successfully applied to various organic electronic devices, such as organic field-effect transistors (OFETs), organic light-emitting diodes (OLEDs), and organic solar cells (OSCs).

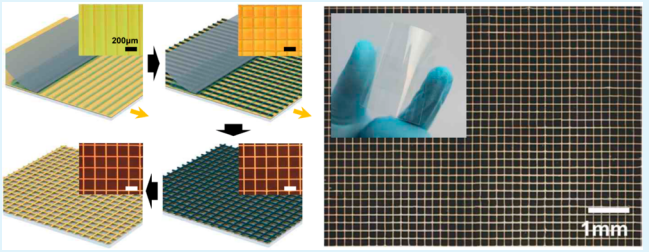

KEYWORDS: *metal grid electrode, evaporative assembly, flow coating, transparent electrode, organic electronic device*

1. INTRODUCTON

Transparent conductors are a key component in a variety of optoelectronic devices, including liquid crystal displays (LCDs),[1,2] organic light emitting diodes (OLEDs),[3,4] organic solar cells (OSCs),[5,6] and touch screens.[7,8] Indium tin oxides (ITOs) are the most widely used transparent conducting materials due to their excellent optical transparency and high electrical conductivity; however, the high cost of ITO, the scarcity of indium, and the fragility of the material present significant drawbacks to the use of ITO in next-generation electronic applications.[7,9] Recent efforts have focused on the development of alternative transparent carbon-based conductors based on carbon nanotubes (CNTs),[10,11] graphene,[7,12−14] or conducting polymers;[15,16] however, the conductivity of such alternative conductors is highly sensitive to the sample fabrication process and is insufficient for many optoelectronic applications. Another class of transparent conductor is derived from metallic nanowires.[9,17−20] Silver nanowire networks,[17,21−23] in particular, have been extensively explored for their potential utility in optoelectronic devices because of their low fabrication costs, high conductivity, transparency, and flexibility; however, silver nanowire networks suffer from several problems, such as the difficulty of developing a uniform nanowire distribution on a substrate, the significant roughness of the networks, inferior electrical contact among the nanowires, and delamination of the nanowires from a substrate. Recently, metallic mesh-type electrodes have also been explored as promising alternatives because both their sheet resistance and their optical transmittance are easily controlled by varying the grid width, spacing, and thickness.[24−29] Another advantage is the reduced junction resistance of the mesh-type structure, which results from the formation of continuous electrical pathway based on the metal grid lines crossing one another. In addition, the work function of the electrode can be simply tuned by changing the metallic materials.

To form metallic grid electrodes, typical methods involve vacuum deposition of metal films followed by the photolithography, nanoimprint lithography (NIL), or transfer printing.[29−31] As an alternative, using of evaporative self-assembly of nanomaterials through flow-coating can be a simple route to form patterns. This method relies on controlling the stick−slip motion at a three-phase (atmosphere−liquid solution−substrate) contact line. Based on the method, the Lin group has demonstrated a wide variety of patterns of

Received: April 13, 2014
Accepted: July 7, 2014
Published: July 7, 2014

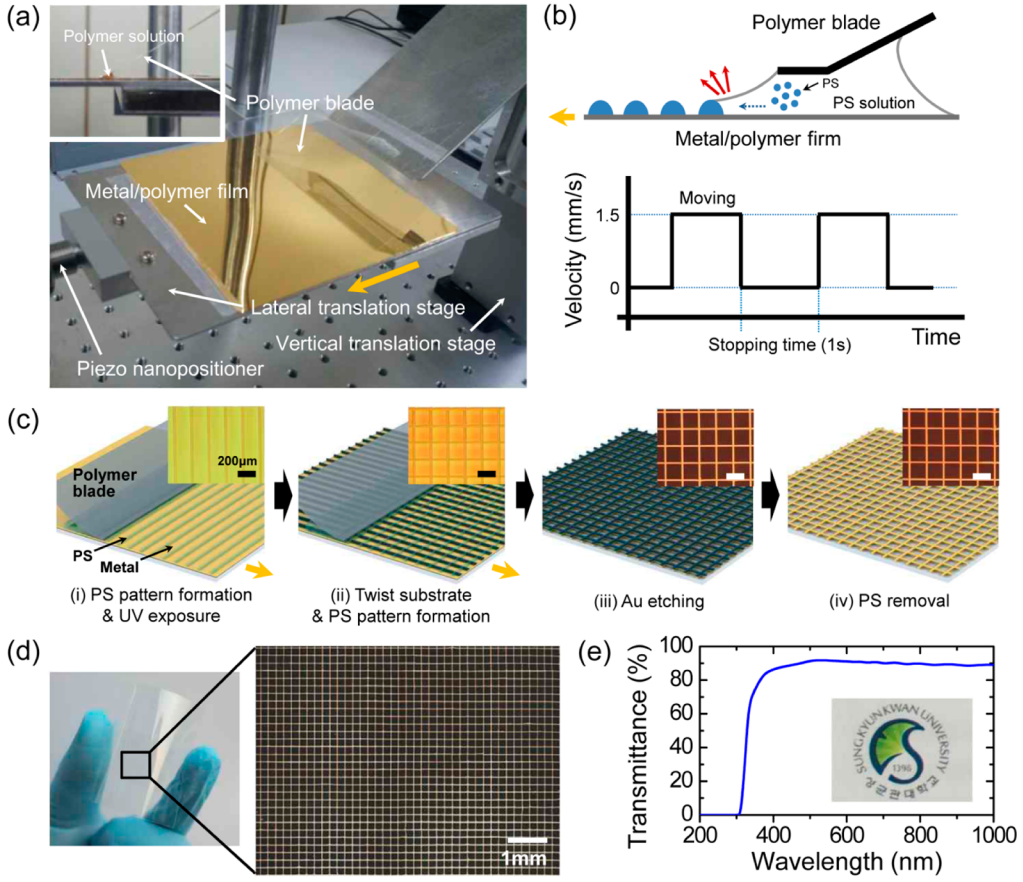

Figure 1. (a) Photographic image of the home-built flow-coating setup. The machine included a lateral translation stage attached to a piezo nanopositioner and a polymer blade attached to a vertical translation stage. The inset shows an enlarged image of the polymer solution trapped by capillary forces between the polymer blade and the substrate. The yellow arrow indicates the direction of motion of the lateral translation stage. (b) Schematic illustration of the formation of the PS line pattern. Lower panel shows the velocity of the linear translation stage as a function of time. (c) Schematic procedure for fabricating the metallic grid electrodes. The process includes (i) forming polymer line patterns on a thermally evaporated metal substrate and exposing the polymer patterns to UV illumination to cross-link the patterned polymer; (ii) polymer line pattern formation on the twisted substrate; (iii) etching away the unprotected metal; (iv) removing the polymer pattern. (d) Photographic and OM images of the flexible transparent Au grid electrodes with a grid width of 4.5 μm and a grid spacing of 200 μm (Au thickness ~90 nm). (e) Optical transmittance as a function of the wavelength. The inset shows an optical image of the Au grid electrodes.

polymers, nanocrystals, nanoparticles, nanorods, and even DNA.[32−34] Also, the Crosby group has recently demonstrated well-aligned patterns of nanoparticles (metallic or semiconducting) by controlling evaporation using a polymeric blade.[35−37] Accordingly, formation of highly uniform metallic grid patterns should be possible through the method. In principle, this method should be readily applied to large area substrates and allow tuning the line width and the spacing of the grid electrodes precisely, despite the avoidance of photolithographic processes but only through careful material selection and tuning processing parameters.

In these lines, we herein demonstrate the fabrication of flexible transparent metallic grid electrodes via evaporative deposition involving flow-coating applicable to the production of various high-performance organic electronic devices. The process included establishing a cross-line pattern of polymers on a metallic film via flow-coating, followed by the removal of both the unprotected metal and residual polymer on the metallic pattern. Metallic grid patterns were prepared with different grid widths and spacings by controlling the concentration of the polymer solution and the moving distance between intermittent stop times of the polymer blade. The optimized Au grid electrodes exhibited an optical transmittance of 92% at 550 nm and a sheet resistance of 97 Ω/sq. The metallic grid electrodes exhibited excellent mechanical flexibility compared to the flexibilities of metallic films and ITO. The metallic grid electrodes were successfully used as electrode materials in various organic electronic devices, such as organic field-effect transistors (OFETs), organic light-emitting diodes (OLEDs), and organic solar cells (OSCs).

2. EXPERIMENTAL SECTION

Fabrication of Metallic Grid Electrode. Polystyrene (PS) solutions having a range of concentrations (1.5−10 mg/mL) were prepared by dissolving PS (M_w = 192 000) in toluene. The solution was stirred for 24 h. All PS solutions were filtered through a polytetrafluoroethylene (PTFE) membrane with a pore size of 0.5 μm prior to flow-coating. A 200 μm thick polyethylene terephthalate (PET) film was cleaned with acetone, isopropanol, and deionized water sequentially, followed by drying under a nitrogen stream. A 90 nm thick Au layer was thermally deposited onto the cleaned PET film.

The flow-coating setup consisted of an angled polymer blade attached to a vertical translation stage and linear translation stage attached to a piezo nanopositioner (Physik Instrumente (PI) GmbH & Co. KG) as shown in Figure 1a. The metal-deposited PET films were fixed on the linear translation stage. A 75 μm thick PET blade that was scored 1.2 mm from the edge was attached rigidly at a 60° angle

relative to the vertical translation stage. The mounting configuration permitted rotational alignment. The PET blade was then brought into contact with the substrate. A PS solution in toluene was then injected between the PET blade and substrate. Due to the capillary forces, the injected solution became trapped at the thinnest regime between the blade and substrate, as shown in Figure 1b. Over a period of time through which the linear translation stage beneath the substrate remained stationary, evaporation of toluene (red arrow in the figure) led migration of nonvolatile PS molecules to the air/solution/substrate contact edge (blue arrow in the figure) and subsequent line deposition of the molecules. As the underneath stage was moved by a certain distance after a given period of time, the meniscus at the air/liquid interface was stretched and the contact angle at this interface was reduced. When the contact angle fell below the critical receding angle, the capillary force exceeded the pinning force and dragged the air/solution/substrate contact edge to a new position. Consequently, the contact angle was recovered to initial value and a new PS line pattern was formed upon subsequent evaporation of toluene. The stop and moving of the linear translation stage were controlled through a homemade software program with variable moving distance, moving velocity, and intermittent stop time.

The transparent and flexible metal grid electrode was fabricated as follows: (i) the PS line patterns were formed on the thermally evaporated Au layer on the PET surface, and UV exposure (254 nm, 28 mW/cm^2, 5 min) cross-linked the PS; (ii) the stage was rotated by 90°, and a second PS line pattern was formed; (iii) the unprotected Au regions were etched with KI (28 Å/s, 20 s); and (iv) the PS grid pattern was removed using reactive ion etching (100 W, 20 sccm, and 60 s). The transmittance and sheet resistance of the Au grid films were characterized by UV−visible spectrophotometry (Agilent 8453) and the four-point probe technique using Keithley 2182A and 6221 units, respectively.

Both sheet resistance (R_s) and optical transmittance ($T_{Au\text{-}grid}$) of the metallic grid electrodes could be estimated from the following equations:[38,39]

$$R_s = \xi \frac{\rho_{Au-grid}}{t_{Au-grid}} \frac{1}{f_F}$$

$$T_{Au-grid} = 100(1 - f_F)^2$$

Here, ξ is a correction factor that can be obtained by fitting the experimental data. $\rho_{Au\text{-}grid}$ is the resistivity of the Au grid. $t_{Au\text{-}grid}$ is the thickness of the Au grid. f_F is the filling factor defined as f_F = W/(D +W), where D and W are grid spacing and width of the electrodes, respectively.

Fabrication of OFETs. Polyethylene terephthalate (PET) coated with indium tin oxide (ITO) (Fine Chemical Industry Inc., Korea) was used as a plastic substrate for fabricating bottom-contact, bottom-gate pentacene FETs. The ITO surface was then cleaned with UV-ozone treatment (254 nm, 28 mW/cm^2) for 30 min. A dimethylformamide solution comprising 10 wt % poly-4-vinylphenol (PVP, M_w = 20,000 g mol^{-1}) and 5 wt % poly(melamine-*co*-formaldehyde) (PMF, M_w = 511 g mol^{-1}) was spin-cast onto an ITO/PET substrate. The substrate was then annealed thermally for 12 h at 80 °C in a vacuum oven to cross-link the polymer. The specific capacitance of the cross-linked PVP (*c*PVP) gate dielectric (thickness = 503 nm) was 7.1 nFcm^{-2}. A Au layer (thickness = 50 nm) was then thermally deposited onto the *c*PVP surface through a shadow mask, followed by the aforementioned patterning steps. The channel length and width were 50 and 1000 μm, respectively. Finally, 50 nm thick pentacene (Aldrich Chemical Co., no purification) films were deposited onto the channel region from a quartz crucible onto the *c*PVP substrates at a rate of 0.2 Ås^{-1} using an organic molecular beam deposition (OMBD) system. The electrical characteristics of the OFETs were measured at room temperature under ambient conditions in a dark environment using Keithley 2400 equipment and 236 source/measure units.

Fabrication of OLEDs. Au grids electrodes with a grid width of 4.5 μm and a grid length of 150 μm were prepared onto polyethylene naphthalate [PEN (thickness = 125 μm), Plastic Films Co., Ltd.]. A PEN substrate coated with ITO (13 Ω/sq) was purchased by Peccell Technologies, Inc. Onto the Au grids electrde, CVD-grown single layer graphene was transferred. Experimental details of the graphene synthesis and transfer was described in Supporting Information. Onto the prepared Au grids, Au grids/graphene, and ITO electrodes, 22 nm thick ZnO were deposited by sputtering. After UV-ozone treatment (254 nm, 28 mW/cm^2) for 10 min, a polyethylene imine (PEI, Sigma-Aldrich) dissolved in 2-methoxyethanol was spin-cast onto ZnO to form 10 nm film and then was dried at 100 °C for 10 min in ambient condition. The substrates were then transferred into a N_2 glovebox, and Super Yellow (Merck OLED Materials. GmbH, catalog number PDY-132) dissolved in toluene (0.9 wt %) was spin-cast onto the PEI layer (thickness of Super Yellow = 230 nm). The structure was then baked at 80 °C for 20 min. The specimen was transferred into a high-vacuum chamber (<10^{-7} Torr). Finally, 5 nm thick MoO_3 (powder, 99.99%, Sigma-Aldrich) and 80 nm thick Ag were deposited by thermal evaporation. The current−voltage−luminance characteristics were measured using a Keithley 236 source measurement unit and a Minolta CS2000 Spectroradiometer.

Fabrication of OSCs. The prepared Au grids, Au grids/graphene, and ITO electrodes were cleaned with acetone, 2-propanol, acetone, and 2-propanol in a sonic bath. UV−ozone treatment was then performed for 10 min. A 200 nm thick PEDOT:PSS (AI4083, Ossila Ltd.) hole conducting layer was spin-cast onto the UV-ozone-treated Au grids, Au grids/graphene, and ITO electrodes (2000 rpm, 1 min). The samples were then baked at 115 °C for 15 min on a hot plate. A bulk heterojunction (BHJ) layer was spin-cast onto the PEDOT:PSS layer. The solution was prepared by dissolving poly({4,8-bis[(2-ethylhexyl)oxy]benzo[1,2-*b*:4,5-b′]dithiophene-2,6-diyl}{3-fluoro-2-[(2-ethylhexyl)carbonyl]thieno[3,4-*b*]thiophenediyl}) (PTB7) and [6,6]-phenyl C_{71} butyric acid methyl ester ($PC_{71}BM$) in a 1:1.5 weight ratio in 3% diiodooctane-containing chlorobenzene solvent. A 6 nm thick TiO_x layer was coated onto the BHJ layer. The TiO_x solution was prepared by adding titanium isopropoxide (TIP) (80 g) into methanol (80 g). Glacial acetic acid (16 g) was then added to the solution. After vigorous stirring for 30 min, 5 mL of water was dropped into the solution. The TiO_x solution was stored at room temperature for over 12 h prior to the spin-coating. Finally, a 100 nm thick Al cathode was thermally evaporated under 10^{-7} Torr. The *J*−*V* performances of the OSCs were measured using an Oriel 91193 (1 kW lamp, 100 mW/cm^2) device, an NREL-calibrated Si solar cell, and Keithley 2400 source meters. A 11.43 mm^2 aperture was used to determine the cell area. The incident photon-to-current efficiency (IPCE) measurements were conducted using a Solar Cell QE/IPCE (Zolix Solar Cell Scan 100).

3. RESULTS AND DISCUSSION

Figure 1a shows photographic images of the flow-coating setup, in which an angled polymer blade is attached to a vertical translation stage and a linear translation stage is attached to a piezo nanopositioner.[36,37] The polyethylene terephthalate (PET) blade was brought into contact with the thermally deposited Au layer (90 nm thick) on a PET substrate. The PET blade was scored 1.2 mm from the edge, which prevented hinging and increased the conformal contact with the substrate, as shown in the inset of Figure 1a and b. A polystyrene (PS) solution was introduced between the PET blade and the substrate and was trapped by capillary forces. When the linear translation stage was stationary over a period of stopping time, the evaporation of toluene (red arrow) induced migration (blue arrow) and deposition of PS near the contact line (upper panel of Figure 1b).[40] Subsequently, the linear translation stage was moved by a certain distance. The movement of the linear translation stage stretched the meniscus until the contact angle fell below the critical receding angle, at which point the capillary force exceeded the pinning force and the contact line slipped to a new position. As a result, the contact angle was

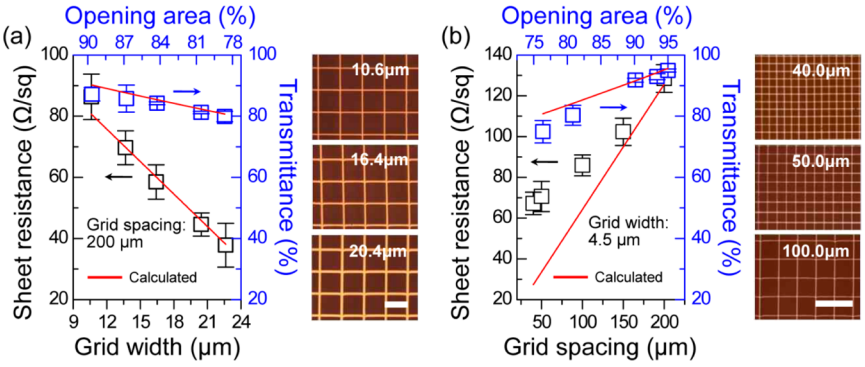

Figure 2. (a) Sheet resistance vs Au grid width and transmittance (at 550 nm) vs opening area. The grid widths were controlled by varying the concentration of the PS solution. The right panel shows representative OM images of the Au grid electrodes prepared with various grid widths. The scale bar indicates 200 μm. (b) Sheet resistance vs Au grid spacing and transmittance (at 550 nm) vs opening area. The grid spacings were controlled by varying the moving distance between intermittent stops. The right panel shows the Au grid electrodes prepared with various grid spacings. The scale bar indicates 200 μm.

recovered to initial value, leaving behind a new PS line. The linear translation stage was moved through a programmed moving distance between intermittent stop times (1 s) at a fixed velocity (1.5 mm/s), as shown in the lower panel of Figure 1b. The line width and spacing could be controlled by varying the stop time and the moving distance, respectively.

A transparent flexible metal grid electrode was fabricated through four essential steps, including (i) PS line pattern formation on the thermally evaporated Au layer mounted on a PET substrate, followed by UV exposure to enable PS cross-linking; (ii) rotation of the stage by 90° and the formation of the second PS line pattern; (iii) etching of the unprotected Au region with KI; and (iv) removal of the residual PS from the Au grid pattern using reactive ion etching (RIE). A schematic diagram and the optical microscopy (OM) images of each step are shown in Figure 1c. Figure 1d shows photographic and OM images of the flexible transparent Au grid electrodes with a grid width of 4.5 and a grid spacing of 200 μm, produced by flow-coating. The optical transmittance of the resulting Au grid electrodes remained nearly constant over the entire visible wavelength range covering 400−800 nm (Figure 1e). The optical transmittance at 550 nm and the sheet resistance were found to be 95% and 128 Ω/sq, respectively.

Both the optical transmittance and the sheet resistance could be controlled by varying the Au grid width and the spacing. First, the Au grid pattern with various grid widths was fabricated by varying the concentration of the PS solution (3, 4, 6, 8, or 10 mg/mL). The moving distance between intermittent stop times (1 s) and the velocity were fixed to 200 μm and 1.5 mm/s, respectively. The grid width increased linearly with the concentration of PS solution, as shown in Supporting Information (SI) Figure S1a. This result could be qualitatively understood in view of the fact that higher concentrations drove more solute toward the edge of the meniscus, resulting in wider lines.[41] The right panel of Figure 2a shows OM images of three representative Au grid electrodes with different grid widths of 10.6, 16.4, and 20.4 μm. The optical transmittance at 550 nm and the sheet resistances of five different samples were measured, as shown in Figure 2a. The sheet resistance decreased linearly as the grid width increased. For example, 10.6 and 22.6 μm grid widths produced sheet resistances of 86 and 38 Ω/sq, respectively. Similarly, the optical transmittance was linearly related to the opening area of the metallic grid electrode; that is, an 87% transmittance was obtained for an 89% opening, and an 80% transmittance was obtained for a 79% opening. The opening area was obtained from the OM images of the patterned grid electrodes. The measured sheet resistance and optical transmittance values agreed well with the calculated values (red lines), indicating the reliable formation of a grid pattern during the flow-coating method. We extended this technique to other metal electrodes, such as Al and Cr, as shown in SI Figure S2.

The grid spacing was controlled by varying the moving distance between the intermittent stops, as shown in Figure 2b. The concentration of PS solution and the velocity were fixed to 1.5 mg/mL and 1.5 mm/s, respectively. The patterned grid spacings (center-to-center) agreed exactly with the programmed distances (right panel in SI Figure S1b). As with the grid width control, the optical transmittance was linearly related to the opening area of the metallic grid electrode. We additionally measured the haze (total diffusion/total transmittance) at 550 nm of the grid electrodes as shown in SI Figure S3, which is superior to the previously reported values of silver nanowire electrodes.[42−45] The sheet resistance increased with the grid spacing, giving a resistance of 67 Ω/sq for a 40 μm grid spacing or 128 Ω/sq for a 200 μm spacing, but unfortunately, large mismatches between the calculated and experimental values were observed for grid spacings of less than 150 μm. Higher values of the measured sheet resistance may incorporate two effects: A PS residue may remain on the metal grid lines after RIE etching, or the metallic line may partially disconnect due to the thin grid width of 4.5 μm. We therefore selected a Au grid of electrodes with an optical transmittance of 92% and a sheet resistance of 97 Ω/sq (a grid width of 4.5 μm and a grid length of 150 μm) for all subsequent electronic applications. This sheet resistance at the fixed transmittance is slightly higher than those of other transparent electrode materials such as ITO, doped metal oxide, and metallic nanowire.[21,46,47] However, the sheet resistance of our grid electrode can be improved by making the grid lines thicker.

The mechanical flexibility and robustness were investigated by measuring the change in the sheet resistances of the Au grid electrodes under compression and tension, such as under a 2.5% strain. The values were compared with those obtained for both the Au bulk film and the commercial ITO electrodes (Figure 3a). The measurement setup is shown in the inset of Figure 3a. The ITO film exhibited a dramatic increase in the sheet resistance at strains beyond 2%; however, both the Au

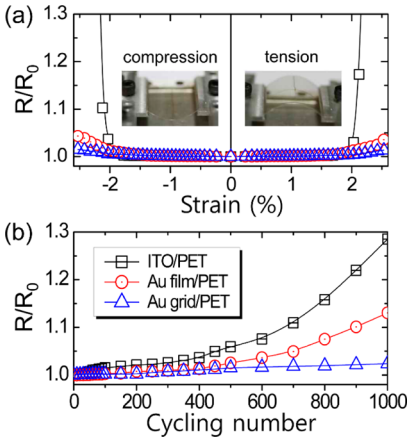

Figure 3. (a) R/R_0 for the ITO, Au film, and Au grid electrodes, as a function of the strain level (±2.5%). The inset shows photographs of the Au grid electrode during compression and tension. (b) R/R_0 as a function of the cycling number during the 1% strain tension.

bulk film and the grid electrode remained stable. A slightly better mechanical stability was observed in the Au grid electrodes beyond a 2% strain. This difference was apparent from the fatigue tests. The sheet resistance of the Au grid electrode was invariant, even after 1000 cycles under a 1% strain along the longitudinal direction (Figure 3b). For open mesh geometries, strains applied in the plane of the substrate may be accommodated by in-plane rotations and distortion of grid mesh without breakage of Au grids.[48]

Flexible transparent Au grid electrodes were successfully used as the electrode materials in a variety of organic electronic devices, including OFETs, OLEDs, and OSCs.

Transparent flexible OFETs bearing Au grid source/drain electrodes were fabricated. Compared with the pad-type electrodes, the utility of the grid electrode in an OFET yielded a larger W/L ratio for a fixed area due to the comb-like geometry. The ITO and cross-linked poly-4-vinylphenol (*c*PVP) were utilized as the gate electrode and gate dielectric, respectively. Source–drain electrodes were prepared by thermally depositing Au onto a *c*PVP surface through a shadow mask, followed by the aforementioned patterning steps (see the inset of Figure 4a). P-type pentacene was thermally deposited onto the channel region. Figure 4a shows the optical transmittance spectra of an OFET array fabricated on a PET substrate over the visible and near-infrared spectral range. The optical transmittance of a neat PET film was 89% at a wavelength of 550 nm. The overall average transparency after fabricating a pentacene FET array on PET was reduced to around 76%. Parts b and c of Figure 4 show typical output and transfer characteristics of the resulting devices, respectively. The device exhibited reasonable gate modulation of I_D in both the linear and saturation regimes (Figure 4b). Our Au grid electrodes resulted in good device performances with a nominal field-effect mobility of 0.43 ± 0.09 $cm^2\ V^{-1}\ s^{-1}$ (using L = 50 μm and W = 1000 μm for calculation) and an on/off current ratio of $\sim 10^5$.[30] While the as-calculated mobility is an overestimate value considering the comb-like geometry of the electrodes (L must be shorter and W must be larger, effectively), it should be noted that that electrodes with larger effective W/L ratio are beneficial for generating higher current level than those made in pad-type.

The transparent flexible Au grid electrodes were next used in inverted OLEDs, as shown in Figure 5a. The basic architecture of the OLED consisted of five layers: an electron injecting ZnO layer, an electron injecting polyethylenimine (PEI) interlayer,[49] an emitting Super Yellow layer, a hole injecting MoO_3 layer, and an Ag anode. Figure 5b shows the current density–voltage–luminance characteristics of the OLEDs prepared using Au grids or Au grids/CVD graphene as the cathode. The results were compared with the properties of a reference OLED prepared with ITO. The device having Au grids alone displayed a higher operating voltage, a lower current density, and a lower luminous efficiency (8.69 cd/A and 1.96 lm/W) than the device prepared with ITO (13.5 cd/A and 5 lm/W). The large electron injection energy barrier from the Au grids (with a work function of ∼5.1 eV) to the ZnO (with a lowest unoccupied molecular orbital, LUMO, energy level of ∼4.4 eV) impeded electron injection and reduced the current density.[50,51] A higher sheet resistance was obtained from the Au grids (97 Ω/sq at 92% at 550 nm) than from the ITO (12 Ω/sq at 90% at 550 nm), which increased the operating voltage and reduced the luminance. On the other hand, the device prepared with Au grids/graphene showed a good current density, luminance, and luminous efficiency (10.1 cd/A and 3.42 lm/W). These values were comparable to those of ITO-based devices. The CVD-grown graphene was n-doped with PEI to reduce the electron injection barrier.[49] The improved performance of the device prepared with graphene (work function of ∼4.6 eV) convincingly demonstrated that a graphene interlayer could effectively reduce the electron injection barrier from the cathode to the electron injection layer, and thus increase the electron injection into the emitting layer. The OLED prepared

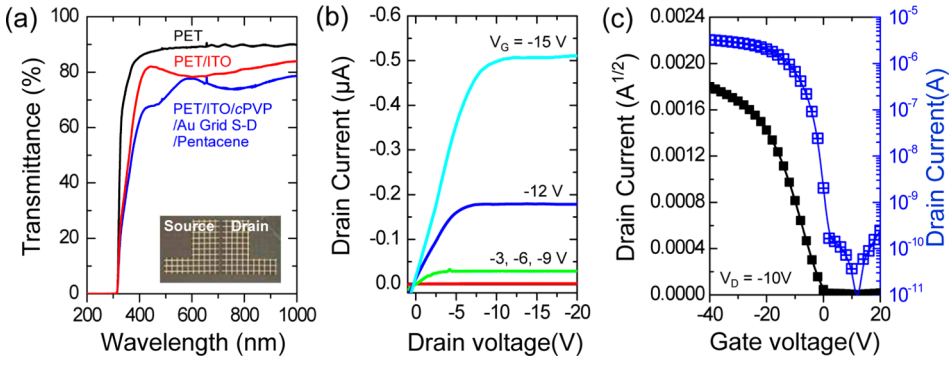

Figure 4. (a) UV–vis spectra of a PET substrate prepared with a pentacene FET array based on Au grid of source/drain electrodes. (b) Output and (c) transfer characteristics of the resulting transparent flexible pentacene FETs.

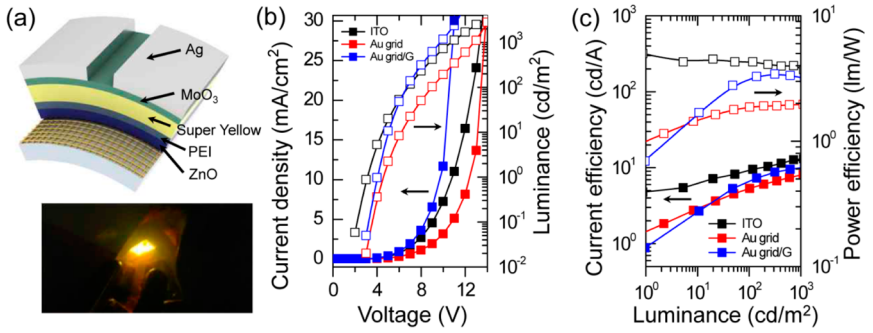

Figure 5. (a) Schematic diagram of the inverted OLED based on the Au grid cathode. The lower panel shows a light emission image of the device under bending. (b) Current density−voltage−luminance characteristics of the OLEDs based on ITO, Au grids, or Au grids/CVD graphene cathodes. (c) The current efficiency and power efficiency as a function of the luminance.

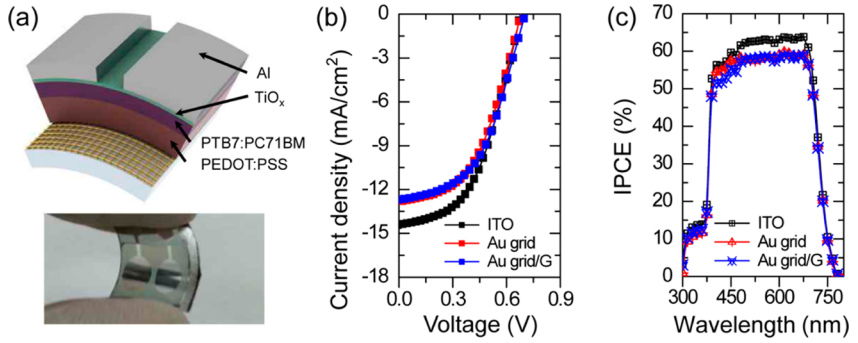

Figure 6. (a) Schematic diagram and photographic image of the OSCs based on Au grid anodes. (b) Photocurrent density−voltage and (c) IPCE−wavelength characteristics of the OSCs based on ITO, Au grids, or Au grids/graphene anodes.

with a Au grid/graphene exhibited a higher current density and luminance at the same fixed voltage, which was better than the performances of devices prepared with ITO due to the lower electron injection barrier; however, the lower transmittance (89% at 550 nm) still blocked some portion of the luminance and thus induced a slightly lower luminous efficiency compared to the ITO device. However, this structure offers a good strategy for preparing air-stable efficient flexible display and lighting devices to replace the more brittle devices based on ITO electrodes.

Finally, the transparent flexible Au grid electrodes were used in OSCs, as shown in Figure 6a. On top of the transparent substrate, a hole-injecting poly(3,4-ethylenedioxythiophene):poly(styrene sulfonic acid) (PEDOT:PSS) layer[52] and a bulk heterojunction PTB7/$PC_{71}BM$ layer were spin-cast, before deposition of an electron extraction TiO_x layer[53] and an Al cathode. Figure 6b shows the photocurrent density−voltage characteristics of OSCs prepared using Au grids or Au grids/CVD graphene as the anode as compared with a reference OSC prepared with ITO. All three electrodes were treated with UV-ozone to enhance the surface wettability and reduce the hole injection barrier. The device prepared with only a Au grid showed a slightly lower short-circuit current (J_{sc}), fill factor (FF), and power conversion efficiency (PCE) (12.9 mA/cm^2, 47.7%, and 4.12%) compared with the values obtained from a device prepared with ITO (14.4 mA/cm^2, 48.0%, and 4.62%). First, the lower transmittance of the Au grids electrode blocked some portion of the incident photons and thus produced a slightly lower J_{sc} compared to that of the ITO device. This result agreed well with the incident photon to electron conversion efficiency (IPCE) spectrum, as shown in Figure 6c. Second, the higher sheet resistance and roughness of the Au grids compared to the ITO lowered the FF. Especially, the high roughness from the grid patterns could induce the morphology of the hole conducting layer to be poor, thereby deteriorating the FF value. On the other hand, the device prepared with Au grids/graphene showed a better open circuit voltage (V_{oc}) of 0.7 V and a FF of 49.1%, comparable to those values obtained from ITO-based devices. The enhanced performance may be due to the improved interfacial properties between the Au grids and the PEDOT:PSS layer as a result of the uniform PEDOT:PSS coating on the graphene.[54] The PCE of the resulting OSCs prepared with the Au grids/graphene anode was 4.38%. Our Au grids/graphene electrodes were successfully used to prepare the anodes in flexible OSCs. Overall, the three basic building units of organic electronics including OFETs, OLEDs, and OSCs assembled with flow-coated flexible metallic grid electrodes exhibited comparable device performances with those made of conventional but brittle ITO electrodes.

4. CONCLUSION

In conclusion, we developed a novel approach to fabricating flexible transparent metallic grid electrodes using a flow-coating method for achieving high-performance organic electronic devices. The electrode grid width and spacing were systematically controlled by varying the concentration of the polymer solution and by programming the distance between the intermittent stop times of the polymer blade, respectively. The resulting Au grid electrodes exhibited an optical transmittance of 92% and a sheet resistance of 97 Ω/sq. Our optimized metallic grid electrodes were successfully used as the electrodes in various organic electronic devices, including OFETs, OLEDs, and OSCs.

■ ASSOCIATED CONTENT

Supporting Information

Experimental detail of graphene synthesis and transfer, grid width vs concentration of PS solution and grid spacing vs slipping distance between intermitent stopping plots (Figure S1), OM images of Al and Cr grid electrodes fabricaed by flow-coating (Figure S2), and haze vs grid width and haze vs grid spacing (Figure S3). This material is available free of charge via the Internet at http://pubs.acs.org/.

■ AUTHOR INFORMATION

Corresponding Author

*Email: jhcho94@skku.edu.

Author Contributions

#J.H.P. and D.Y.L. contributed equally this work.

Notes

The authors declare no competing financial interest.

■ ACKNOWLEDGMENTS

This work was supported by the KANEKA/SKKU Incubation Center and financially supported by Kaneka Corp. in Japan, the Center for Advanced Soft-Electronics funded by the Ministry of Science, ICT and Future Planning as Global Frontier Project (2013M3A6A5073177), Basic Science Research Program (2009-0083540) of the National Research Foundation of Korea (NRF) funded by the Ministry of Education, Science and Technology, and the World-Class 300 Project (Development of organic materials with high transmittance, high insulating properties, and high flexibility for next generation display) funded by the Small and Medium Business Administration (SMBA) in Korea.

■ REFERENCES

(1) Blake, P.; Brimicombe, P. D.; Nair, R. R.; Booth, T. J.; Jiang, D.; Schedin, F.; Ponomarenko, L. A.; Morozov, S. V.; Gleeson, H. F.; Hill, E. W.; Geim, A. K.; Novoselov, K. S. Graphene-Based Liquid Crystal Device. *Nano Lett.* **2008**, *8*, 1704−1708.

(2) Hecht, D. S.; Hu, L.; Irvin, G. Emerging Transparent Electrodes Based on Thin Films of Carbon Nanotubes, Graphene, and Metallic Nanostructures. *Adv. Mater.* **2011**, *23*, 1482−1513.

(3) Han, T. H.; Lee, Y.; Choi, M.-R.; Woo, S. H.; Bae, S. H.; Hong, B. H.; Ahn, J. H.; Lee, T. W. Extremely Efficient Flexible Organic Light-Emitting Diodes with Modified Graphene Anode. *Nat. Photonics* **2012**, *6*, 105−110.

(4) Bansal, M.; Srivastava, R.; Lal, C.; Kamalasanan, M.; Tanwar, L. Carbon Nanotube-Based Organic Light Emitting Diodes. *Nanoscale* **2009**, *1*, 317−330.

(5) Wang, X.; Zhi, L.; Tsao, N.; Tomović, Ž.; Li, J.; Müllen, K. Transparent Carbon Films as Electrodes in Organic Solar Cells. *Angew. Chem., Int. Ed.* **2008**, *120*, 3032−3034.

(6) Chen, C. C.; Dou, L.; Zhu, R.; Chung, C. H.; Song, T. B.; Zheng, Y. B.; Hawks, S.; Li, G.; Weiss, P. S.; Yang, Y. Visibly Transparent Polymer Solar Cells Produced by Solution Processing. *ACS Nano* **2012**, *6*, 7185−7190.

(7) Bae, S.; Kim, H.; Lee, Y.; Xu, X.; Park, J. S.; Zheng, Y.; Balakrishnan, J.; Lei, T.; Kim, H. R.; Song, Y. I.; Kim, Y. J.; Kim, K. S.; Ozyilmaz, B.; Ahn, J. H.; Hong, B. H.; Iijima, S. Roll-to-Roll Production of 30-Inch Graphene Films for Transparent Electrodes. *Nat. Nanotechnol.* **2010**, *5*, 574−578.

(8) Wang, J.; Liang, M.; Fang, Y.; Qiu, T.; Zhang, J.; Zhi, L. Rod-Coating: Towards Large-Area Fabrication of Uniform Reduced Graphene Oxide Films for Flexible Touch Screens. *Adv. Mater.* **2012**, *24*, 2874−2878.

(9) Lee, J. Y.; Connor, S. T.; Cui, Y.; Peumans, P. Solution-Processed Metal Nanowire Mesh Transparent Electrodes. *Nano Lett.* **2008**, *8*, 689−692.

(10) Wu, Z.; Chen, Z.; Du, X.; Logan, J. M.; Sippel, J.; Nikolou, M.; Kamaras, K.; Reynolds, J. R.; Tanner, D. B.; Hebard, A. F.; Rinzler, A. G. Transparent, Conductive Carbon Nanotube Films. *Science* **2004**, *305*, 1273−1276.

(11) Tenent, R. C.; Barnes, T. M.; Bergeson, J. D.; Ferguson, A. J.; To, B.; Gedvilas, L. M.; Heben, M. J.; Blackburn, J. L. Ultrasmooth, Large-Area, High-Uniformity, Conductive Transparent Single-Walled-Carbon-Nanotube Films for Photovoltaics Produced by Ultrasonic Spraying. *Adv. Mater.* **2009**, *21*, 3210−3216.

(12) Wu, J.; Becerril, H. A.; Bao, Z.; Liu, Z.; Chen, Y.; Peumans, P. Organic Solar Cells with Solution-Processed Graphene Transparent Electrodes. *Appl. Phys. Lett.* **2008**, *92*, 263302.

(13) Kim, K. S.; Zhao, Y.; Jang, H.; Lee, S. Y.; Kim, J. M.; Kim, K. S.; Ahn, J. H.; Kim, P.; Choi, J. Y.; Hong, B. H. Large-Scale Pattern Growth of Graphene Films for Stretchable Transparent Electrodes. *Nature* **2009**, *457*, 706−710.

(14) Kalita, G.; Matsushima, M.; Uchida, H.; Wakita, K.; Umeno, M. Graphene Constructed Carbon Thin Films as Transparent Electrodes for Solar Cell Applications. *J. Mater. Chem.* **2010**, *20*, 9713−9717.

(15) Kim, W.; Mäkinen, A.; Nikolov, N.; Shashidhar, R.; Kim, H.; Kafafi, Z. Molecular Organic Light-Emitting Diodes Using Highly Conducting Polymers as Anodes. *Appl. Phys. Lett.* **2002**, *80*, 3844−3846.

(16) Shin, S.; Yang, M.; Guo, L. J.; Youn, H. Roll-to-Roll Cohesive, Coated, Flexible, High-Efficiency Polymer Light-Emitting Diodes Utilizing ITO-Free Polymer Anodes. *Small.* **2013**, *9*, 4036−4044.

(17) Hu, L.; Kim, H. S.; Lee, J.-Y.; Peumans, P.; Cui, Y. Scalable Coating and Properties of Transparent, Flexible, Silver Nanowire Electrodes. *ACS Nano* **2010**, *4*, 2955−2963.

(18) Kang, M. G.; Joon Park, H.; Hyun Ahn, S.; Jay Guo, L. Transparent Cu Nanowire Mesh Electrode on Flexible Substrates Fabricated by Transfer Printing and Its Application in Organic Solar Cells. *Sol. Energy Mater. Sol. Cells.* **2010**, *94*, 1179−1184.

(19) Sánchez-Iglesias, A.; Rivas-Murias, B.; Grzelczak, M.; Pérez-Juste, J.; Liz-Marzán, L. M.; Rivadulla, F.; Correa-Duarte, M. A. Highly Transparent and Conductive Films of Densely Aligned Ultrathin Au Nanowire Monolayers. *Nano Lett.* **2012**, *12*, 6066−6070.

(20) Hsu, P. C.; Wang, S.; Wu, H.; Narasimhan, V. K.; Kong, D.; Lee, H. R.; Cui, Y. Performance Enhancement of Metal Nanowire Transparent Conducting Electrodes by Mesoscale Metal Wires. *Nat. Commun.* **2013**, *4*, 2522.

(21) Wu, H.; Menon, M.; Gates, E.; Balasubramanian, A.; Bettinger, C. J. Reconfigurable Topography for Rapid Solution Processing of Transparent Conductors. *Adv. Mater.* **2013**, *5*, 706−711.

(22) Van de Groep, J.; Spinelli, P.; Polman, A. Transparent Conducting Silver Nanowire Networks. *Nano Lett.* **2012**, *12*, 3138−3144.

(23) Xu, F.; Zhu, Y. Highly Conductive and Stretchable Silver Nanowire Conductors. *Adv. Mater.* **2012**, *24*, 5117−5122.

(24) Ho, X.; Lu, H.; Liu, W.; Tey, J. N.; Cheng, C. K.; Kok, E.; Wei, J. Electrical and Optical Properties of Hybrid Transparent Electrodes That Use Metal Grids and Graphene Films. *J. Mater. Res.* **2013**, *28*, 620−626.

(25) Higashitani, K.; McNamee, C. E.; Nakayama, M. Formation of Large-Scale Flexible Transparent Conductive Films Using Evaporative Migration Characteristics of Au Nanoparticles. *Langmuir* **2011**, *27*, 2080−2083.

(26) Zou, J.; Yip, H. L.; Hau, S. K.; Jen, A. K. Y. Metal Grid/Conducting Polymer Hybrid Transparent Electrode for Inverted Polymer Solar Cells. *Appl. Phys. Lett.* **2010**, *96*, 203301.

(27) Hong, S.; Yeo, J.; Kim, G.; Kim, D.; Lee, H.; Kwon, J.; Lee, H.; Lee, P.; Ko, S. H. Nonvacuum, Maskless Fabrication of a Flexible Metal Grid Transparent Conductor by Low-Temperature Selective Laser Sintering of Nanoparticle Ink. *ACS Nano* **2013**, *7*, 5024−5031.

(28) Zhu, Y.; Sun, Z.; Yan, Z.; Jin, Z.; Tour, J. M. Rational Design of Hybrid Graphene Films for High-Performance Transparent Electrodes. *ACS Nano* **2011**, *5*, 6472−6479.
(29) Jin, Y.; Cheng, Y.; Deng, D.; Jiang, C.; Qi, T.; Yang, D.; Xiao, F. Site-Selective Growth of Patterned Silver Grid Networks as Flexible Transparent Conductive Film by Using Poly (Dopamine) at Room Temperature. *ACS Appl. Mater. Interfaces.* **2014**, *6*, 1447−1453.
(30) Jung, S.; Lee, S.; Song, M.; Kim, D. G.; You, D. S.; Kim, J. K.; Kim, C. S.; Kim, T. M.; Kim, K. H.; Kim, J. J.; Kang, J. W. Extremely Flexible Transparent Conducting Electrodes for Organic Devices. *Adv. Energy Mater.* **2014**, *4*, 1−8.
(31) Lee, K.; Kim, S.; Jeong, H.; Pak, Y.; Song, H.; Park, J.; Lim, K.; Kim, J.; Kim, Y. S.; Ko, H. C.; Kwon, I. K.; Jung, G. All-Solution-Processed Transparent Thin Film Transistor and Its Application to Liquid Crystal Driving. *Adv. Mater.* **2013**, *25*, 3209−3214.
(32) Li, B.; Han, W.; Jiang, B.; Lin, Z. Crafting Threads of Diblock Copolymer Micelles Via Flow-Enabled Self-Assembly. *ACS Nano* **2014**, *8*, 2936−2942.
(33) Li, B.; Han, W.; Byun, M.; Zhu, L.; Zou, Q.; Lin, Z. Macroscopic Highly Aligned DNA Nanowires Created by Controlled Evaporative Self-Assembly. *ACS Nano* **2013**, *7*, 4326−4333.
(34) Xu, J.; Xia, J.; Lin, Z. Evaporation-Induced Self-Assembly of Nanoparticles from a Sphere-on-Flat Geometry. *Angew. Chem., Int. Ed.* **2007**, *119*, 1892−1895.
(35) Lawrence, J.; Pham, J. T.; Lee, D. Y.; Liu, Y.; Crosby, A. J.; Emrick, T. Highly Conductive Ribbons Prepared by Stick−Slip Assembly of Organosoluble Gold Nanoparticles. *ACS Nano* **2014**, *8*, 1173−1179.
(36) Lee, D. Y.; Pham, J. T.; Lawrence, J.; Lee, C. H.; Parkos, C.; Emrick, T.; Crosby, A. J. Macroscopic Nanoparticle Ribbons and Fabrics. *Adv. Mater.* **2013**, *25*, 1248−1253.
(37) Kim, H. S.; Lee, C. H.; Sudeep, P.; Emrick, T.; Crosby, A. J. Nanoparticle Stripes, Grids, and Ribbons Produced by Flow Coating. *Adv. Mater.* **2010**, *22*, 4600−4604.
(38) Ghosh, D.; Chen, T.; Pruneri, V. High Figure-of-Merit Ultrathin Metal Transparent Electrodes Incorporating a Conductive Grid. *Appl. Phys. Lett.* **2010**, *96*, 041109.
(39) Jang, Y.; Kim, J.; Byun, D. Invisible Metal-Grid Transparent Electrode Prepared by Electrohydrodynamic (EHD) Jet Printing. *J. Phys. D: Appl. Phys.* **2013**, *46*, 155103.
(40) Deegan, R. D.; Bakajin, O.; Dupont, T. F.; Huber, G.; Nagel, S. R.; Witten, T. A. Capillary Flow as the Cause of Ring Stains from Dried Liquid Drops. *Nature.* **1997**, *389*, 827−829.
(41) Stafford, C. M.; Roskov, K. E.; Epps, T. H., III; Fasolka, M. J. Generating Thickness Gradients of Thin Polymer Films Via Flow Coating. *Rev. Sci. Instrum.* **2006**, *77*, 023908.
(42) Hwang, J. H.; Park, T. H.; Lee, H. J.; Choi, K. B.; Park, Y. W.; Ju, B. K. Low-Haze Light Extraction from Organic Light-Emitting Diode Lighting with Auxiliary Electrode by Selective Microlens Arrays. *Opt. Lett.* **2013**, *38*, 4182−4185.
(43) Caputo, D.; de Cesare, G.; Irrera, F.; Palma, F. Solar-Blind Uv Photodetectors for Large Area Applications. *IEEE Trans. Electron Devices* **1996**, *43*, 1351−1356.
(44) Langley, D.; Giusti, G.; Mayousse, C.; Celle, C.; Bellet, D.; Simonato, J. P. Flexible Transparent Conductive Materials Based on Silver Nanowire Networks: A Review. *Nanotechnology* **2013**, *24*, 452001.
(45) Kumar, A. K.; Bae, C. W.; Piao, L.; Kim, S. H. Silver Nanowire Based Flexible Electrodes with Improved Properties: High Conductivity, Transparency, Adhesion, and Low Haze. *Mater. Res. Bull.* **2013**, *48*, 2944−2949.
(46) Joseph, B.; Manoj, P.; Vaidyan, V. Studies on the Structural, Electrical, and Optical Properties of Al-Doped Zno Thin Films Prepared by Chemical Spray Deposition. *Ceram. Int.* **2006**, *32*, 487−493.
(47) Liu, C. H.; Yu, X. Silver Nanowire-Based Transparent, Flexible, and Conductive Thin Film. *Nanoscale Res. Lett.* **2011**, *6*, 75.
(48) Jang, H. Y.; Lee, S. K.; Cho, S. H.; Ahn, J. H.; Park, S. Fabrication of Metallic Nanomesh: Pt Nano-Mesh as a Proof of Concept for Stretchable and Transparent Electrodes. *Chem. Mater.* **2013**, *25*, 3535−3538.
(49) Zhou, Y.; Fuentes-Hernandez, C.; Shim, J.; Meyer, J.; Giordano, A. J.; Li, H.; Winget, P.; Papadopoulos, T.; Cheun, H.; Kim, J.; Fenoll, M.; Dindar, A.; Haske, W.; Najafabadi, E.; Khan, T. M.; Sojoudi, H.; Barlow, S.; Graham, S.; Brédas, J. L.; Marder, S. R.; Kahn, A.; Kippelen, B. A Universal Method to Produce Low−Work Function Electrodes for Organic Electronics. *Science* **2012**, *336*, 327−332.
(50) Lee, B. R.; Choi, H.; Park, J. S.; Lee, H. J.; Kim, S. O.; Kim, J. Y.; Song, M. H. Surface Modification of Metal Oxide Using Ionic Liquid Molecules in Hybrid Organic−Inorganic Optoelectronic Devices. *J. Mater. Chem.* **2011**, *21*, 2051−2053.
(51) Kabra, D.; Lu, L. P.; Song, M. H.; Snaith, H. J.; Friend, R. H. Efficient Single-Layer Polymer Light-Emitting Diodes. *Adv. Mater.* **2010**, *22*, 3194−3198.
(52) Kim, W.; Kim, N.; Kim, J. K.; Park, I.; Choi, Y. S.; Wang, D. H.; Chae, H.; Park, J. H. Polymer Bulk Heterojunction Solar Cells with PEDOT:PSS Bilayer Structure as Hole Extraction Layer. *ChemSusChem* **2013**, *6*, 1070−1075.
(53) Wang, D. H.; Kim, J. K.; Seo, J. H.; Park, I.; Hong, B. H.; Park, J. H.; Heeger, A. J. Transferable Graphene Oxide by Stamping Nanotechnology: Electron-Transport Layer for Efficient Bulk-Heterojunction Solar Cells. *Angew. Chem., Int. Ed.* **2013**, *52*, 2874−2880.
(54) Kim, H.; Bae, S. H.; Han, T. H.; Lim, K. G.; Ahn, J. H.; Lee, T. W. Organic Solar Cells Using Cvd-Grown Graphene Electrodes. *Nanotechnology* **2014**, *25*, 014012.